CRYSTALLOGRAPHY REPORTS, 2025, Vol. 70, No. 1, pp. 34–39

PHYSICAL PROPERTIES OF CRYSTALS

ZnO MICROTUBES: FORMATION MECHANISM AND WHISPERING-GALLERY MODE LASING

© 2025 A. P. Tarasov*, L. A. Zadorozhnaya, B. V. Nabatov, and V. M. Kanevsky

Shubnikov Institute of Crystallography, Kurchatov Complex of Crystallography and Photonics, National Research Center "Kurchatov Institute", Moscow, Russia

**e-mail: tarasov.a@crys.ras.ru*

Received November 04, 2024
Revised November 19, 2024
Accepted November 19, 2024

Abstract. The luminescent and laser properties of ZnO microtubes synthesized by a modified thermal evaporation method were studied using photoluminescence spectroscopy. It was shown that whispering gallery modes are responsible for lasing in the near UV range. The possibility of achieving low lasing thresholds (down to ~ 8 kW/cm^2) and high optical quality factors (over 3900) was demonstrated. A mechanism for the formation of such microcrystals was proposed, based on the assumption of simultaneous growth and etching along the [0001] crystallographic direction.

DOI: 10.31857/S00234761250105e4

INTRODUCTION

Zinc oxide ZnO is a wide-bandgap semiconductor that is widely used in scientific research and industry [1, 2]. One of the areas of application of ZnO is optoelectronic technologies due to its optical, electronic and scintillation properties [3–8]. In particular, ZnO is considered a promising basis for UV lasers, including micro- and nanolasers [3, 9–11]. Among such devices, the most efficient in terms of laser thresholds and optical quality factors are whispering gallery mode (**WGM**) microlasers [12, 13]. The simplest way to implement such devices is to synthesize microcrystals with hexagonal geometry, such as microwhiskers, micropyramids, microdisks, polyhedral microcrystals, demonstrating light amplification and laser effect immediately after synthesis without additional post-growth treatment [12–18]. Among all the morphologies of such microcrystals, the most frequently studied are morphologies with a clearly expressed crystallographic direction [0001]. Examples of these are microrods and microwhiskers.

Microcrystals with such morphology can be obtained by various methods, among which the most popular is the gas transport synthesis method [12]. In [19, 20], the possibility of synthesizing these structures by the pyrolytic carbothermal synthesis (**PCS**) method developed at the A.V. Shubnikov Institute of Crystallography of the Russian Academy of Sciences was demonstrated [21, 22]. In this case, it was possible to synthesize fairly large microrods with a diameter of up to 20 μm, supporting WGM lasing. PCS is essentially a modification of the thermal evaporation method; it retains many of the advantages of this method, including the relative simplicity and safety of synthesis. At the same time, it provides wide opportunities for the production of structures with various morphologies, including powders [22], films [23], and microcrystals on substrates [19, 20].

In this paper, we demonstrate the possibility of synthesizing microtubes (hollow or "negative" microrods) with WGM using the PCS method. It is shown that such microstructures can have not only low laser thresholds [24], but also high optical quality factors.

METHODS AND MATERIALS

ZnO microtubes were synthesized on sapphire (0001) substrates using the PCS method. Zinc granules with a purity of 99.999% (Alfa Aesar, USA) were used as a precursor. The synthesis was carried out in a corundum crucible for 30 min at a temperature of 1050°C. In general, the synthesis parameters were similar to those used previously for the growth of ZnO microrods with a relatively small diameter of 1–6 μm [25], but the sample was located closer to the window in the crucible, which was a source of oxygen.

Microscopic studies were performed using a Jeol JSM-6000PLUS scanning electron microscope (**SEM**). Photoluminescence (**PL**) of the structure was studied at room temperature using low-intensity quasi-continuous optical excitation (xenon lamp flash frequency of 80 Hz) and relatively powerful pulsed optical excitation. In the first case, a Varian Cary Eclipse spectrofluorimeter equipped with a xenon lamp and a photomultiplier tube was used, while radiation with a wavelength of 315 nm was used to excite PL. High-intensity excitation was

achieved by exposure to the third harmonic of a Nd:YAG laser providing pulsed radiation with a wavelength of 355 nm, a repetition rate of 15 Hz, and a pulse duration of 10 ns. The excitation spot diameter on the sample was ~100 μm. In the latter case, the PL registration (both of individual microtubes and their arrays) was carried out using an MDR-206 monochromator combined with a photoelectron multiplier. The geometry of the experiment corresponded to earlier studies of ZnO microrods [19, 25].

DISCUSSION OF RESULTS

Fig. 1 shows a micrograph of one of the synthesized ZnO microtubes. The microtubes are rods 40–60 μm long with a narrow base, a thicker upper part, and a cavity in it. The average diameter of the upper part is ~10 μm. In general, the synthesized microcrystals are similar in morphology to those obtained previously [25], but are characterized by larger sizes, which is apparently due to a large influx of oxygen.

The area of the sample near its edge with an array of microtubes was selected for the study (insert in Fig. 1). Electron microscopic studies of this area indicate that cavities are present in all microcrystals with a diameter greater than 6–7 μm.

In [24], where ZnO microtubes were also obtained from the gas phase, the following mechanism for the formation of such microcrystals is suggested. Crystal growth occurs mainly in the [0001] direction as a result of the self-catalytic vapor–liquid–solid process, when a zinc droplet serves both as a nucleus and a growth catalyst. In this case, the oxide initially overgrows the lateral surfaces of the droplet, which ultimately leads to the formation of a core–shell Zn/ZnO rod structure. Then Zn, having a relatively low melting point (~419.5°C), evaporates from the (0001) surface, which leads to the formation of a microtube.

However, after studying the SEM image of the samples obtained by the PCS method, another mechanism for the formation of negative (hollow) ZnO microcrystals seems to be the most probable. In addition to the fact that metallic Zn belongs to the group of low-melting metals, it is quite volatile (the evaporation temperature is 906 °C at atmospheric pressure). Due to this, under PCS conditions, a concentration of Zn vapor sufficient for its deposition on the surface of already grown or growing microcrystals – microrods can easily be achieved. This occurs if the mass of zinc reacting with oxygen is less than the mass of excess Zn, in which case metallic zinc will continue to condense during synthesis, but at a lower rate, while the size of liquid zinc droplets on the ends of growing microcrystals will increase. At a fairly high crystallization temperature (950-1050 °C), irregular oval-shaped formations are clearly visible on the surface of already grown relatively small microcrystals at the cooling stage (Fig. 2a).

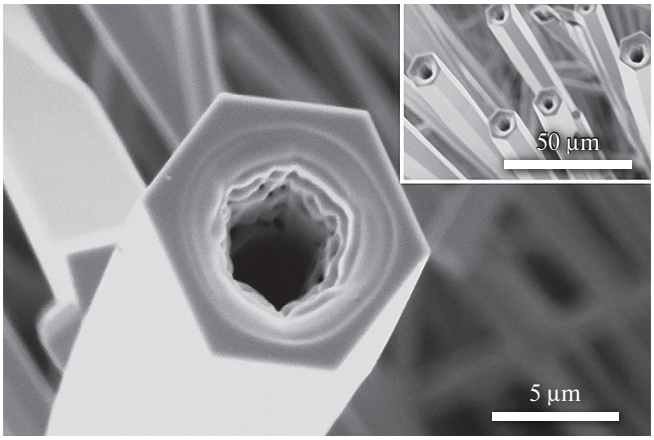

Fig. 1. SEM image of a ZnO microtube (the inset shows an array of microtubes).

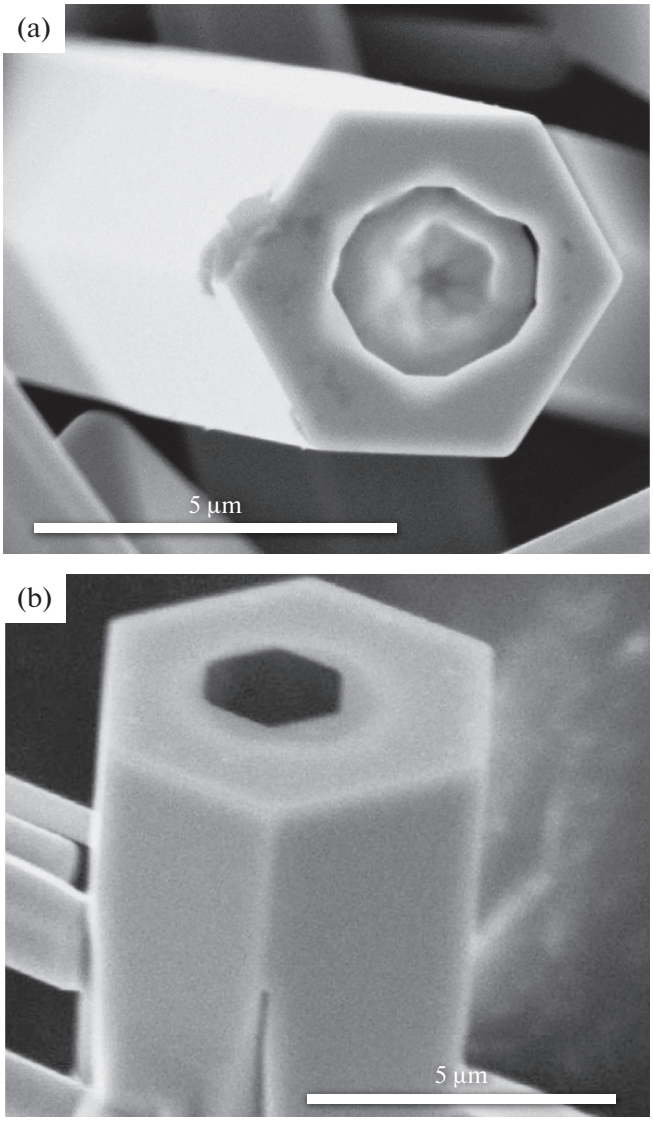

Fig. 2. SEM images of ZnO microrods: a – the beginning of the etching process of the microrod from the surface side (0001), b – the formation of a hexagonal pit on the end of the microrod.

A droplet of ZnO–Zn alloy on the (0001) face of a microrod serves as a site of preferential gas etching in accordance with the solid–liquid–vapor mechanism (this mechanism was proposed in [26] as the reverse of the vapor–liquid–solid growth mechanism). This droplet penetrates into the crystal, in accordance with the symmetry of the (0001) face. As a result, a hexagonal pit with a flat bottom is almost always formed at the end of the microrod, not necessarily in the center of the end (Fig. 2b). It is believed that such pits are caused by impurity inclusions [27], in contrast to pointed pits associated with dislocations [28]. In this case, along with foreign elements, an impurity here should be understood as an excess of a component of the crystallized compound and the components of the gas mixture during chemical vapor deposition. Thus, excess Zn in the gas environment acts as a native (own) impurity, initiating the process of crystal evaporation.

Fig. 3 shows the PL spectra of the microtube array recorded under low-intensity quasi-continuous excitation (a) and pulsed laser excitation with a relatively low power density ρ_{exc} ~ 6 kW/cm^2 (b). Several differences can be seen in the obtained spectra. First of all, a different number of emission bands is observed. While the spectrum in Fig. 3b shows two emission bands – in the near UV and visible parts of the spectrum, the spectrum in Fig. 3a contains only the visible luminescence band. In this case, the parameters of the visible luminescence band – the position (λ_m) and the width at half maximum (FWHM) – are approximately the same: in the case of continuous excitation, λ_m and FWHM are 516 and 117 nm, respectively; under pulsed excitation, these parameters are 518 and 119 nm. The position λ_m and the half-width FWHM of the UV band in the spectrum in Fig. 3b are 393 and 17 nm, respectively. This band is known as the near-band-edge emission of ZnO. In this case, the UV band itself clearly consists of several components: a short-wave shoulder is observed near the main maximum in the region of ~380 nm (insert in Fig. 3b).

Studies of ZnO microstructures carried out at different temperatures [29, 30] allow us to understand the mechanisms of microtube luminescence. Thus, the emission with a maximum in the region of 380 nm is caused mainly by the first phonon replica of the recombination emission of a free exciton. The main band with a maximum at 393 nm is associated with the scattering of excitons on free electrons. This is confirmed by further studies of the behavior of near-band-edge emission at different levels of photoexcitation. The band of visible (green) emission is caused by transitions involving deep energy levels in the forbidden band of ZnO, associated with defects of the crystal lattice, mainly oxygen vacancies in different charge states [31, 32].

The absence of near-band-edge luminescence at low-intensity excitation may be due to the bending of energy bands due to the existence of excess charge on the semiconductor surface. Such bending promotes the formation of a depleted layer and spatial separation of electrons and holes formed as a result of excitation, which prevents their radiative recombination [33]. At sufficiently powerful excitation, a large number of created carriers leads to the neutralization of excess surface charge and, as a consequence, to the straightening of energy bands. As a result, the probability of recombination with the emission of a photon increases. An increase in the excitation level also leads to the saturation of visible luminescence centers [34] and, consequently, to a relative increase in near-band-edge emission.

To study the laser effect in individual microtubes, some of the crystals were scraped off onto a clean silicon substrate. The microcrystal was then isolated from the other crystals under a microscope using a thin needle. Fig. 4a shows the evolution of the near-band-edge

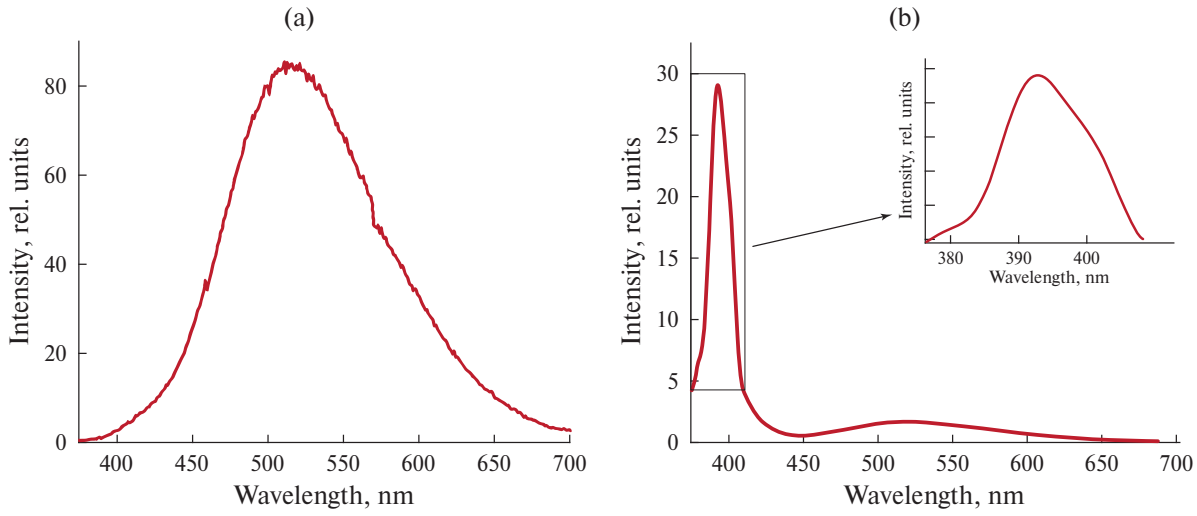

Fig. 3. PL spectra of an array of ZnO microtubes recorded under low-intensity quasi-continuous excitation (a) and pulsed laser excitation with a power density ρ_{exc} ~ 6 kW/cm^2 (b).

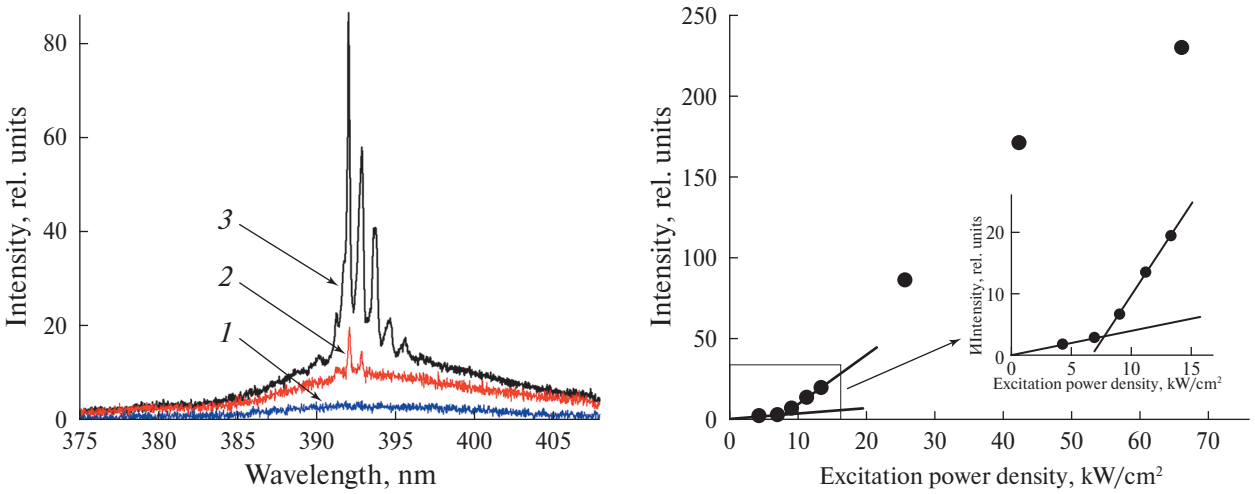

Fig. 4. Near-band-edge emission spectra of a ZnO microtube at different excitation power densities ρ_{exc}: *1* – 7, *2* – 13, *3* – 26 kW/cm² (a); dependence of intensity on ρ_{exc} in the region of the most intense laser line with a wavelength of ~ 392.05 nm (b).

emission spectra of one of these microtubes with increasing power density ρ_{exc} of pulsed laser excitation. At a relatively low excitation level with ρ_{exc} = 7 kW/ cm², the spectrum is represented by a spontaneous emission band similar to that described earlier (Fig. 3b). As ρ_{exc} increases above 8–9 kW/cm², narrow lines appear in the spectrum in the region of the maximum of the luminescent band, the intensity of which rapidly increases with increasing ρ_{exc}. As the excitation level increases, new lines appear mainly in the long-wavelength part of the UV spectrum. With increasing ρ_{exc}, the intensity of the lines grows faster than the intensity of the spontaneous luminescence band. This is reflected in Fig. 4b showing the dependence of intensity on ρ_{exc} in the region of the most intense laser line with a wavelength of ~392.05 nm. The graph shows a sharp break at ρ_{exc} ~ 8 kW/cm², which corresponds to the threshold of the laser effect in the microtube.

In general, the studied microstructure demonstrates not only low laser thresholds, but also high optical quality factors. Thus, Fig. 5 shows the lasing spectrum of one of the microcrystals at ρ_{exc} ~ 0.1 MW/cm². Taking into account the spectral position (392–393 nm) and FWHM (0.1 nm) of individual laser lines, we obtain a quality factor of more than 3900. This value is comparable and often even higher than in the case of other high-quality ZnO-based microcrystalline lasers with WGMs [10, 11, 14, 19, 35].

In ZnO microcrystals, laser effect is observed with the participation of two main types of optical modes – Fabry–Perot modes (**FPM**) and WGM. The dispersion of the refractive index in the near UV range for ZnO microcrystals synthesized by the PCS method is determined by the expression [19, 36]:

$$n(\lambda) = \left(A + \frac{B\lambda^2}{\lambda^2 - C^2} + \frac{D\lambda^2}{\lambda^2 - E^2} \right)^{0.5}, \qquad (1)$$

where the parameters are: $A = 4.693$, $B = 0.197$, $C = 176.06$, $D = 0.0435$, $E = 375.99$.

The length L of a FPM resonator can be estimated using the formula:

$$L = \frac{\lambda^2}{2\Delta\lambda\left(n(\lambda) - \lambda dn/d\lambda\right)}, \qquad (2)$$

where $\Delta\lambda$ is the distance between adjacent laser lines [37]. Considering that in the case under study $\Delta\lambda$ = 0.8–1 nm, the estimate using formula (2) yields L = 15–19 μm, which is less than the lengths of the microtubes.

On the other hand, estimates using the planar hexagonal WGM resonator model indicate that the observed spectral pattern corresponds to the laser effect on the WGMs. According to this model, the wavelength of the WGM with number N is determined by the expression:

$$\lambda_{WGM} = \frac{1.5\sqrt{3}n(\lambda)D}{N + \frac{6}{\pi}\tan^{-1}\left(n(\lambda)\sqrt{3n(\lambda)^2 - 4}\right)}, \qquad (3)$$

where D is the diameter of the hexagonal resonator [12, 38]. In this case, we consider only TE-type modes, since TM-modes in the near-band-edge region are usually much weaker [39, 40]. For simplicity, we assume that the cavity in the microcrystal does not affect the wavelength of the modes (3). Using (3), we find the diameter of the microtube corresponding to the spectrum in Fig. 5. To do this, three types of lines must be combined on one graph of the $\lambda(D)$ dependence: lines according to formula (3) for different N, horizontal lines corresponding to the experimentally observed positions of the laser lines, and a vertical line corresponding to a certain diameter. In Fig. 6, such a graph is constructed for N in the range of 179–188. The most accurate intersection of the lines is achieved at a diameter of

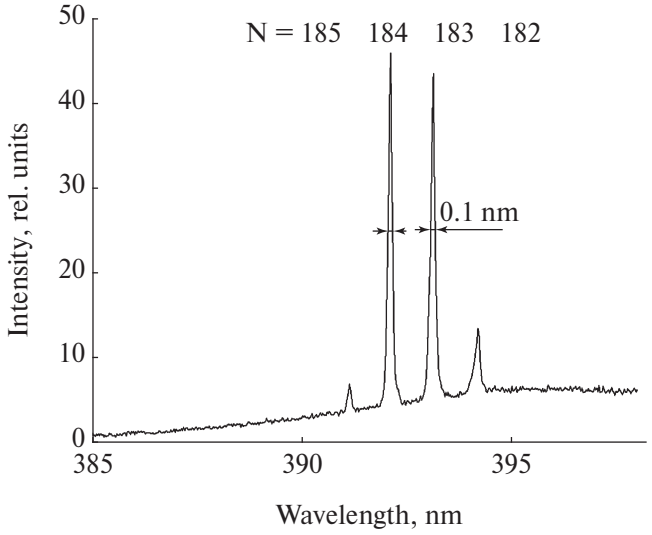

Fig. 5. Lasing spectrum of one of the ZnO microtubes at ρ_{exc} ~ 0.1 MW/cm^2.

~12.05 μm, which corresponds to the diameters of the upper part of the studied microtubes. In this case, the mode numbers corresponding to the laser lines are 185, 184, 183, 182. They are also shown in Fig. 5.

The occurrence of laser effect in the region of 392–394 nm and the intense red shift of the lasing region with increasing pump level also indicate the formation of gain on the WGMs [29]. In this case, the gain mechanism is exciton-electron scattering, which can occur in optically and geometrically high-quality ZnO microcrystals at room temperature.

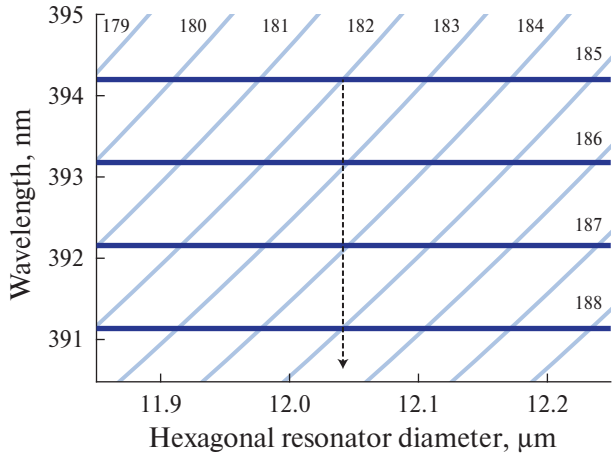

Fig. 6. The $\lambda_{WGM}(D)$ dependence simulated using formula (3) for WGMs with TE polarization (oblique curves) and the experimentally recorded spectral positions of laser lines (horizontal lines) according to Fig. 5. The arrow corresponds to the diameter D at which the most accurate coincidence of the positions of laser lines and neighboring TE modes is observed.

CONCLUSION

The radiative properties of ZnO microtubes in the near UV and visible wavelength ranges are investigated. The microtubes are synthesized by the pyrolytic carbothermal synthesis method, which is essentially a modification of the thermal evaporation method. Differences in the luminescence spectra of the structure at different photoexcitation levels are revealed and interpreted. The possibility of exciting lasing on whispering gallery modes in individual microtubes in the near UV region is shown. In this case, it is possible to achieve extremely low laser thresholds — down to 8 kW/cm^2 and sufficiently high optical quality factors — over 3900. It is noted that optical gain is provided by the process of excitons scattering on free electrons.

ACKNOWLEDGMENTS

The authors express their gratitude to I.S. Volchkov for assistance in conducting SEM studies of the samples.

FUNDING

The study was supported by the grant of the Russian Science Foundation (grant No. 23-29-00535, https://rscf.ru/en/project/23-29-00535/) and carried out using the equipment of Shared Research Center “Structural diagnostics of materials”.

CONFLICT OF INTERESTS

The authors declare that they have no conflicts of interest.

REFERENCES

1. *Morkoc H., Ozgur U.* Zinc oxide: fundamentals, materials and device technology. Weinheim: Wiley-VCH, 2009.
2. *Sharma D.K., Shukla S., Sharma K.K., Kumar V.* // Mater. Today. 2022. V. 49. P. 3028. https://doi.org/10.1016/j.matpr.2020.10.238
3. *Klingshirn C.F.* Semiconductor Optics. Berlin: Springer, 2012.
4. *Srivastava V., Gusain D., Sharma Y.C.* // Ceram. Int. 2013. V. 39. P. 9803. https://doi.org/10.1016/j.ceramint.2013.04.110
5. *Oprea O., Andronescu E., Ficai D. et al.* // Curr. Org. Chem. 2014. V. 18. P. 192.
6. *Uikey P., Vishwakarma K.* // Int. J. Emerg. Tech. Comp. Sci. Electron. 2016. V. 21. P. 239.
7. *Di Mauro A., Fragalà M.E., Privitera V., Impellizzeri G.* // Mater. Sci. Semicond. Process. 2017. V. 69. P. 44. https://doi.org/10.1016/j.mssp.2017.03.029
8. *Tarasov A.P., Venevtsev I.D., Muslimov A.E. et al.* // Quantum Electron. 2021. V. 51. P. 366. https://doi.org/10.1070/QEL17534

9. *Znaidi L., Illia G.S, Benyahia S. et al.* // Thin Solid Films. 2003. V. 428. P. 257. https://doi.org/10.1016/S0040-6090(02)01219-1
10. *Dong H., Zhou B., Li J. et al.* // J. Materiomics. 2017. V. 3. P. 255. https://doi.org/10.1016/j.jmat.2017.06.001
11. *Tashiro A., Adachi Y., Uchino T.* // J. Appl. Phys. 2023. V. 133. P. 221101. https://doi.org/10.1063/5.0142719
12. *Xu C., Dai J., Zhu G. et al.* // Las. Photon. Rev. 2014. V. 8. P. 469. https://doi.org/10.1002/lpor.20130012
13. *Yang Y.D., Tang M., Wang F.L. et al.* // Photonics Res. 2019. V. 7. P. 594. https://doi.org/10.1364/PRJ.7.000594
14. *Chen R., Ling B., Sun X.W., Sun H.D.* // Adv. Mater. 2011. V. 23. P. 2199. https://doi.org/10.1002/adma.201100423
15. *Michalsky T., Wille M., Dietrich C.P. et al.* // Appl. Phys. Lett. 2014. V. 105. P. 211106. https://doi.org/10.1063/1.4902898
16. *Qin F., Xu C., Lei D.Y. et al.* // ACS Photonics. 2018. V. 5. P. 2313. https://doi.org/10.1021/acsphotonics.8b00128
17. *Tarasov A.P., Muslimov A.E., Kanevsky V.M.* // Photonics. 2022. V. 9. P. 871. https://doi.org/10.3390/photonics9110871
18. *Tarasov A.P., Zadorozhnaya L.A., Muslimov A.E. et al.* // JETP Lett. 2021. V. 114. P. 517. https://doi.org/10.1134/S0021364021210116
19. *Tarasov A.P., Lavrikov A.S., Zadorozhnaya L.A., Kanevsky V.M.* // JETP Lett. 2022. V. 115. P. 502. https://doi.org/10.1134/S0021364022100514
20. *Tarasov A.P., Zadorozhnaya L.A., Kanevsky V.M.* // J. Appl. Phys. 2024. V. 136. P. 073102. https://doi.org/10.1063/5.0214420
21. *Li L.E., Demianets L.N.* // Opt. Mater. 2008. V. 30. P. 1074. https://doi.org/10.1016/j.optmat.2007.05.013
22. *Demyanets L.N., Li L.E., Lavrikov A.S., Nikitin S.V.* // Crystallogr. Rep. 2010. V. 55. P. 142. https://doi.org/10.1134/S1063774510010219
23. *Zadorozhnaya L.A., Tarasov A.P., Lavrikov A.S., Kanevsky V.M.* // Comp. Opt. 2024. V. 48. P. 696. https://doi.org/10.18287/2412-6179-CO-1414
24. *Dong H., Sun L., Xie W. et al.* // J. Phys. Chem. C. 2010. V. 114. P. 17369. https://doi.org/10.1021/jp1047908
25. *Tarasov A.P., Zadorozhnaya L.A., Kanevsky V.M.* // JETP Lett. 2024. V. 119. P. 903. https://doi.org/10.1134/S0021364024601519
26. *Wagner R.S.* // J. Crystal Growth. 1968. V. 3/4. P. 159.
27. *Kaldis E.* // Crystal Growth and Characterization. Amsterdam: North Holland, 1975.
28. *Sharma R.B.* // J. Appl. Phys. 1970. V. 41. P. 1866. https://doi.org/10.1063/1.1659122
29. *Tarasov A.P., Muslimov A.E., Kanevsky V.M.* // Materials. 2022. V. 15. P. 8723. https://doi.org/10.3390/ma15248723
30. *Tarasov A.P., Ismailov A.M., Gadzhiev M.K. et al.* // Photonics. 2023. V. 10. P. 1354. https://doi.org/10.3390/photonics10121354
31. *Ozgur U., Alivov Y.I., Liu C. et al.* // J. Appl. Phys. 2005. V. 98. P. 41301. https://doi.org/10.1063/1.1992666
32. *Ghosh M., Ningthoujam R.S., Vatsa R.K. et al.* // J. Appl. Phys. 2011. V. 110. P. 054309. https://doi.org/10.1063/1.3632059
33. *Zhang Z., Yates Jr. J.T.* // Chem. Rev. 2012. V. 112. P. 5520. https://doi.org/10.1021/cr3000626
34. *Guo B., Qiu Z.R., Wong K.S.* // Appl. Phys. Lett. 2003. V. 82. P. 2290. https://doi.org/10.1063/1.1566482
35. *Dai J., Xu C.X., Wu P. et al.* // Appl. Phys. Lett. 2010. V. 97. P. 011101. https://doi.org/10.1063/1.3460281
36. *Tarasov A.P., Briskina Ch.M., Markushev V.M. et al.* // JETP Lett. 2019. V. 110. P. 739. https://doi.org/10.1134/S0021364019230115
37. *Zimmler M.A., Bao J., Capasso F. et al.* // Appl. Phys. Lett. 2008. V. 93. P. 051101. https://doi.org/10.1063/1.2965797
38. *Czekalla C., Sturm C., Schmidt-Grund R. et al.* // Appl. Phys. Lett. 2008. V. 92. P. 241102. https://doi.org/10.1063/1.2946660
39. *Wiersig J.* // Phys. Rev. A. 2003. V. 67. P. 023807. https://doi.org/10.1103/PhysRevA.67.023807
40. *Liu J., Lee S., Ahn Y. et al.* // Appl. Phys. Lett. 2008. V. 92. P. 263102. https://doi.org/10.1063/1.2952763